Magnetization experiments on frozen ferrofluids

2004 J. Phys.: Condens. Matter 16 427

(http://iopscience.iop.org/0953-8984/16/3/019)

INSTITUTE OF PHYSICS PUBLISHING JOURNAL OF PHYSICS: CONDENSED MATTER

J. Phys.: Condens. Matter **16** (2004) 427–443 PII: S0953-8984(04)70038-7

Magnetization experiments on frozen ferrofluids

O Michele[1], J Hesse[1], H Bremers[1], E K Polychroniadis[2], K G Efthimiadis[2] and H Ahlers[3]

[1] Institut für Metallphysik und Nukleare Festkörperphysik, Technische Universität, Mendelssohnstraße 3, 38106 Braunschweig, Germany
[2] Department of Physics, Aristotle University of Thessaloniki, GR 54006 Thessaloniki, Greece
[3] Physikalisch-Technische Bundesanstalt, Bundesallee 100, 38116 Braunschweig, Germany

E-mail: O.Michele@tu-bs.de

Received 7 October 2003
Published 9 January 2004
Online at stacks.iop.org/JPhysCM/16/427 (DOI: 10.1088/0953-8984/16/3/019)

Abstract

Ensembles consisting of Co nanoparticles fixed in space by freezing ferrofluids are investigated. In frozen ferrofluids a well defined low temperature magnetic state of the nanoparticle system can be achieved. We distinguish between textured samples (preferred orientation of easy axes) and non-textured with randomly oriented easy axes. Considering the magnetization curves of such systems bears in principle the possibility to distinguish between influences arising from particle anisotropy and particle–particle interaction. Our intention is to present new experimental strategies aiming to separate these influences from magnetization measurements versus temperature. In another approach we analysed the susceptibility derived from magnetization measurements and determined the mean magnetic moment of the particles and an additional field which may be caused by the anisotropy of the particles or the interaction between them. Transmission electron microscopy was used for the direct measurement of the particles' sizes and their size distribution.

1. Introduction

In recent years magnetic nanosized single-domain particle systems have become of general interest because of their continuously increasing range of applications. These start with the well known problem of enhancing the capacity of magnetic data storage devices and end with bacteria and organic molecules used for medical marking or local application of medicine. Our aim is to investigate the magnetic properties from the basic physical point of view and derive as much information as possible from new strategies in performing magnetization experiments.

Small particles can be prepared e.g. as powder by ball milling, in bulk material by stepwise annealing of amorphous ribbons (Hupe *et al* 1999), as layer by a plasma–gas-condensation process (Peng *et al* 2002) or as more or less free particles in ferrofluids by wet chemical reactions.

Ferrofluids after their first synthesis in the middle of the 1960s (see Neuringer and Rosensweig 1964) became rather popular in many technical applications (e.g. ferrofluids may be used in magnetic seals and valves or as damping material in loud-speakers) and for basic physical investigations (Bakuzis *et al* 2000, Fannin *et al* 1988). Ferrofluids can be made from Co, Fe, Fe_3O_4, Ni and various compounds (hereby specifying the particles' crystal-anisotropy and Zeeman energy). They consist of small particles coated by some kind of organic hull, preventing the particles from agglomerating. In the carrier fluid the particles may move freely.

Many papers have been published dealing with the magnetic and rheological properties of ferrofluids since their first synthesis: in 1980 Zahn and Shenton published the 'Magnetic fluids biography' with over 800 references. In 1997 Blums *et al* reported the results presented in the recent past in a book covering more than 600 citations. A broad overview over measurement techniques applicable to ferrofluids is shown by Pathmamanoharan and Philipse (1998). Among other experiments they performed electron microscopy, small angle x-ray scattering, powder diffraction, viscosimetry, infrared spectroscopy and magnetization measurements. The value of magnetization and susceptibility measurements for the understanding of relaxational processes in small particle systems is shown by Fannin (2002) and references herein.

From the very beginning, ferrofluids attracted researchers due to the possibility to study the magnetic behaviour of single-domain particle systems in the liquid and frozen states. For example, Luo *et al* (1991) studied the influence of dipole interaction versus the random anisotropy in a frozen ferrofluid. Williams *et al* (1993) found that liquid ferrofluids obey the universal Langevin B/T-behaviour whereas frozen ferrofluids destroy this universality due to the particle-inherent anisotropy.

Ferrofluids are still attractive systems due to the possibility of manipulating the magnetic particles in different ways; i.e. by dilution the mean distance may be changed and so influences of particle–particle interactions can be studied. A magnetic field can be applied to the ferrofluid before or after the freezing of the carrier liquid.

In a recent paper, Hesse *et al* (2002) showed that it is possible to 'transform' the magnetic behaviour of various small particle systems consisting of fixed-in-space magnetic single-domain particles into a quasi-paramagnetic. This means that each particle's magnetic moment exhibits a component in the direction of the applied magnetic field. Then it is possible to apply the Langevin super-paramagnetism formalism to describe the behaviour of such a system in a rather good approximation.

Our aim is to consider the magnetic behaviour of single-domain particle ensembles which fulfil the condition that the system behaviour is in good approximation determined by the single-particle properties. That means the particle–particle interaction is weak enough to prevent collective behaviour of the ensemble. Such collective behaviour might be the phenomenon of self-organization which needs a suitable particle–particle interaction or domain formation in such a nanoparticle system or the mutual influence on the dynamic behaviour (see for example Chantrell *et al* 1982, Eberbeck and Ahlers 1999, Denisov *et al* 2000, Hansen and Mørup 1998).

In this contribution we investigate a custom Co-based ferrofluid by SQUID magnetometry and electron microscopy. The magnetization measurements of interest were made in the frozen state (temperature below the melting point of the carrier liquid) but after preparing the low temperature magnetic state of the particle system in different but well defined ways. We will try to derive the magnetic characteristics as mean magnetic moment of the particles and also a measure for the interaction energy being a property of the ensemble.

2. The investigated particle system: electron microscopy

First, we would like to introduce the system under consideration in this paper: we deal with custom Co-based ferrofluids produced by the Berlin Heart AG, Berlin. The preparation process

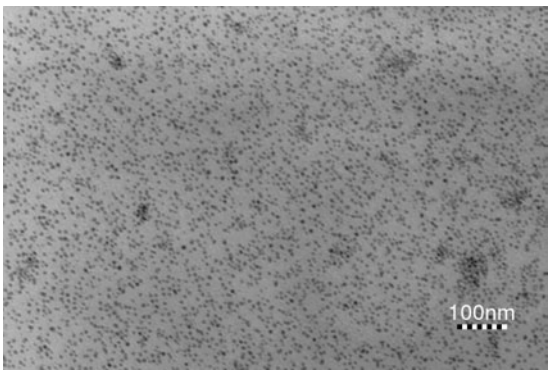

Figure 1. TEM image of a Co-based ferrofluid in the dried state with original magnification of 46 100.

is published by Berkov *et al* (2000). The ferrofluids consist of fine particles in the order of 4 nm radius and a carrier liquid which is used as a solvent. As usual the particles have an organic hull which prevents them from agglomerating. In our case the carrier liquid is made from clean petroleum; its freezing or melting temperature is about 140 K. To get a first glance at the system, TEM measurements in a JEOL JEM 120 CX with 120 kV operating voltage were made to get the size distribution of the nanoparticles and the least possible distance between the particles, which is determined by their organic hull.

For TEM the samples were prepared in the following manner: a drop of highly diluted ferrofluid was allowed to dry on a special copper grid coated with SiO. Different samples with different concentrations were prepared and examined in the electron microscope. All images showed well separated spherical particles and no indications for agglomeration to big clusters were found (figure 1). The organic hull (thickness approximately 1 nm, material AOT ($C_{20}H_{37}NaO_7S$)) maintains a minimum distance of the particles. The images were scanned into a computer and the particle sizes were estimated by counting the pixels of each particle. The automatic analysis included more than 12 000 particles from several images and regions of the samples.

One can try to fit a log normal distribution to the particle radii r achieved by the histogram method (figure 2). The function and the parameters used are

$$f(x) = \frac{1}{x\sigma\sqrt{2\pi}} \exp\left(-\frac{(\ln x - \kappa)^2}{2\sigma^2}\right) \tag{1}$$

$$\overline{x} = \frac{\overline{r}}{r_0} = \exp\left(\kappa + \frac{\sigma^2}{2}\right) \tag{2}$$

$$\frac{S^2}{S_0^2} = (\exp\sigma^2 - 1)\exp(2\kappa + \sigma^2) \tag{3}$$

where $f(x)$ is the function to fit to the experimental data via the parameters κ and σ. $\overline{r}$ is the expectation value of the distribution and S is a scale for the width of the distribution (S_0 and r_0 represent the unit 1 nm).

This distribution is frequently used for nanoparticle size distributions (Koksharov 2000). The mean radius of the particles evaluated from electron microscopy (figure 1) is $\overline{r} = 3.7$ nm with a distribution width of $S = 0.6$ nm. This rather small value indicates a narrow distribution.

Co nanoparticles tend to oxidize on their surface. Due to the smallness of the particles, the volume fraction of 'the surface' is rather high. In our case, we think of a Co oxide shell with

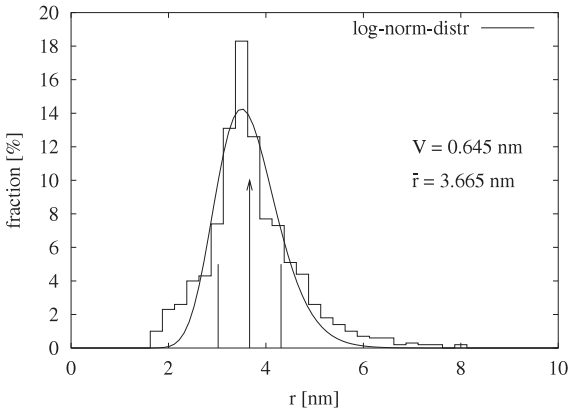

Figure 2. Radius distribution of the nanoparticles (steps) achieved from TEM images and a fit by a log normal distribution. The parameters of the distribution are indicated. The arrow on the figure shows the expectation value $\overline{r}$ and the lines left and right indicate the S-value for the width of the fitted distribution.

an average thickness of 1 nm on the particle's Co core (we compared the magnetic moment distribution derived with the formalism described by Weser and Stierstadt (1985) (sum of Langevin functions combined with the Tichonov regularization mechanism) with the results from electron microscopy). The magnetic moment of the Co oxide is much smaller than that of bulk cobalt. The Co oxide influences the magnetic behaviour of the particles (e.g. see Stamps 2002, Kachkachi *et al* 2000): the magnetic moment of the particles is reduced (so-called dead layer concept) and the Co oxide surface induces an additional surface anisotropy.

3. Different cooling sequences for magnetization measurements on ferrofluids

In the present work we focus on different ways of performing magnetization measurements on ferrofluids. We describe these possibilities and in table 1 we focus on the sequences we use in this contribution. Our ferrofluids are liquid at room temperature and become frozen around 140 K. We prepared different low temperature magnetic states (LTMSs) by using varying cooling sequences and measured the magnetization during warming the sample with a defined heating rate of 3 K min^{-1} in small fields B_{FW}. In the temperature range 5–140 K the particles are fixed in the frozen liquid and the Brownian relaxation is suppressed (Brown 1963, Abu-Aljarayesh *et al* 2002), but the Néel relaxation is still possible (Néel 1949). Above 140 K the particles may rotate and move more or less freely following the temperature dependence of the carrier liquid's viscosity. For the presentation of the possibilities to prepare LTMSs we consider non-interacting free-standing particles that do not agglomerate in high fields when the petroleum is liquid. This is why the following description has an ideal character. In the discussion we will not neglect these effects but partly use them for the explanation of our measurements.

In the following we present the cooling sequences and their abbreviations used in the experiments. The '/' indicates a change of the magnetic field during the cooling sequence at $T = 140$ K. The '//' indicates the break between cooling and warming the sample (usually at $T = 5$ K). At all break-points the temperature is well below the melting point of the carrier liquid. We show that the orientation of the particles' easy directions and the orientation of the magnetization vectors can be prepared separately. All the cooling sequences described below lead to a well defined and reproducible LTMS. When we talk about 'high fields', we compare the anisotropy energy of the particles KV with the Zeeman energy M_0BV (K is the anisotropy

constant, M_0 the saturation magnetization, V the particle volume and B the external magnetic field). Typical fields corresponding to the blocking energies are in the range of 100 mT. We prepare our LTMS with high fields of 2 T so that we can be sure to overcome all energy barriers (even the energy barriers of big particles).

Cooling sequences are as follows.

ZFC//FW (zero-field cooling, field warming). The sample is cooled with $B = 0$ from room temperature to 5 K. The particles' easy axes are randomly distributed in the liquid and become frozen in this orientation. The same is true for the magnetization vectors of the particles. For the field warming (FW) a small field B_{FW} is applied (for all measurements performed B_{FW} is in the range of 3–100 mT). During FW the temperature is increased from 5 to 300 K at a definite rate.

PHFC//FW (positive high field cooling, field warming). The sample is cooled with $B = 2$ T from room temperature to 5 K. The particles align their easy axes with the external field B and are fixed in space below 140 K. This kind of preparation leads to a textured sample. The magnetization vectors of the particles align parallel to the field B. During the FW (5–300 K) a small field B_{FW} is applied and the magnetization is recorded.

ZFC/PHFC//FW (zero-field cooling, positive high field cooling, field warming). The sample is cooled from room temperature to 140 K with $B = 0$; after freezing of the ferrofluid at 140 K the external field is increased to $B = 2$ T. With this field the temperature is lowered to 5 K. The result is that the easy axes are randomly distributed, but the magnetization vectors have a positive projection on the measurement direction defined by the applied external positive magnetic field. We call this state quasi-paramagnetic because this procedure removes the blocking behaviour for all particles. During the FW (5–300 K) a small field B_{FW} is applied.

ZFC/FC//FW (zero-field cooling, field cooling, field warming). The sample is cooled with $B = 0$ from room temperature to 140 K. At 140 K the external field strength later used for field warming $B = B_{\mathrm{FW}}$ is applied. With this field the temperature is lowered to 5 K. The result is that the easy axes are nearly randomly distributed and the magnetization vectors of the particles are oriented in such a manner that the sample is near the equilibrium state for this external field B. During the FW (5–300 K) the same field B_{FW} is active. This procedure is described very often in the literature. Its disadvantage is that during FW some undefined numbers of particles must overcome their blocking energy. This 'mixture' of magnetization directions makes it difficult (if not impossible) to interpret the measurements.

NHFC//FW (negative high field cooling, field warming). The sample is cooled with $B = -2$ T from room temperature to 5 K (the minus indicates that the field points against the later measurement direction). The particles are aligned with their easy axes parallel to the external field B. The system becomes textured. All magnetization vectors have a negative projection on the measurement direction. For the time of FW (5–300 K) a small positive field B_{FW} is applied. The advantage of this procedure is that all particles must overcome their maximum blocking energy during FW.

ZFC/NHFC//FW (zero-field cooling, negative high field cooling, field warming). The sample is cooled from room temperature to 140 K with $B = 0$; the sample remains untextured. At 140 K the external field is increased to $B = -2$ T. With this field the temperature is lowered to 5 K. This results in a random distribution of the easy axes and a negative projection on the measurement direction of the magnetization vectors. During the FW (5–300 K) the field B_{FW} is applied. The advantage of this procedure is that all particles must overcome their blocking energies.

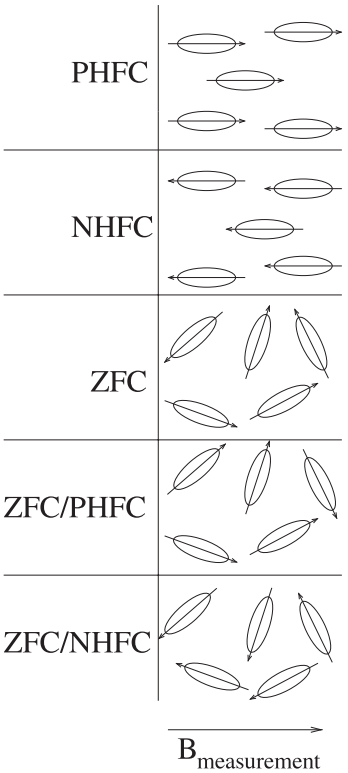

Figure 3. Two-dimensional model of different well defined low temperature magnetic states for five nanoparticles after various cooling sequences: for cooling sequences starting in high fields (positive or negative) the particles tend to align to the external field (textured sample) and so do the magnetization vectors of the particles. For cooling sequences starting with ZFC (non-textured sample) the easy axes are randomly distributed.

From this overview, it can be seen that there exist two generally different sample states: the textured state where all easy axes are aligned with the external field B and the case where the easy axes of the particles are randomly distributed and non-textured all over the sample. In addition, the direction of the magnetization vectors relative to the particles' easy axes can be prepared separately after freezing of the carrier liquid. Table 1 shows a short overview of the measurement procedures used in this contribution. Additionally they can be visualized (see figure 3 for a 'five-particle model' of the LTMS) in a two-dimensional model of single-domain particles with uniaxial anisotropy (Stoner and Wohlfarth 1948). The long axes of the ellipses show the easy axes of the (uniaxial) anisotropy. The arrows indicate the magnetization direction for the whole particle (single domain).

4. Magnetization measurements and discussion

In this section examples of measurements performed with the new strategies described above are presented. The procedures in question are summarized in a short form in table 1.

Three samples of the same Co ferrofluid were investigated: non-diluted (Co100), diluted by adding 5.77 weight parts of petroleum (Co103) and diluted by adding 49.9 parts of petroleum (Co104). Because in the SQUID magnetometer a plastic vessel as sample holder with fixed ferrofluid volume was used, a decrease of the samples' magnetization with dilution was

Table 1. Procedures to prepare different low temperature magnetic states (LTMSs) used in this contribution. The melting point of the liquid is at about 140 K and defines the temperature below which the particles cannot move or turn. B_{FW} is between 3 and 100 mT.

Abbreviation	Measuring procedure	Expected LTMS
ZFC//FW	300 K $\xrightarrow{B=0\ \mathrm{T}}$ 5 K; 5 K $\xrightarrow{B_{FW}}$ 300 K	Randomly orientated easy axes and magnetization vectors
PHFC//FW	300 K $\xrightarrow{B=2\ \mathrm{T}}$ 5 K; 5 K $\xrightarrow{B_{FW}}$ 300 K	Textured (the particles' easy axes are aligned with B), saturated in positive direction
ZFC/PHFC//FW	300 K $\xrightarrow{B=0\ \mathrm{T}}$ 140 K, 140 K $\xrightarrow{B=2\ \mathrm{T}}$ 5 K; 5 K $\xrightarrow{B_{FW}}$ 300 K	Random orientation of easy axes but aligned magnetization vectors
ZFC/NHFC//FW	300 K $\xrightarrow{B=0\ \mathrm{T}}$ 140 K, 140 K $\xrightarrow{B=-2\ \mathrm{T}}$ 5 K; 5 K $\xrightarrow{B_{FW}}$ 300 K	Random orientation of easy axes but aligned magnetization vectors

Table 2. The properties of the prepared and measured samples.

Sample	Dilution	M (5 K, 2 T) (10^{-3} emu)	m (mg)	M/m (emu g^{-1})
Co100	1:1	1074	28.03	38.3
Co103	1:(1+5.77)	78.98	23.93	3.30
Co104	1:(1+49.9)	13.119	23.91	0.55

observed. Table 2 summarizes the properties of the three samples (magnetization M taken at $T = 5$ K and $B = 2$ T, m the mass of the ferrofluid and M/m the mass normalized magnetization). The units are indicated in the table. The idea of diluting assumes a dipole–dipole interaction between the particles which is in its isotropic part proportional $1/d^3$ or $1/v_p$ where d is the mean particle–particle distance and v_p the volume belonging (in the mean) to one particle.

The influence on the FW curve ($B_{FW} = 50$ mT) of the different cooling sequences used can be seen in the next figures. Because we expect the lowest influence of particle–particle interaction in the most diluted (Co104) ferrofluid we start by presenting the results achieved for this sample.

In figure 4 the FW magnetization is shown starting from three different LTMSs prepared in the non-textured sample (ZFC//FW, ZFC/NHFC//FW, ZFC/PHFC//FW). The external field for FW is $B_{FW} = 50$ mT.

The magnetization curves start (depending on the LTMS) at zero, high negative or high positive magnetization. The magnetization curves lead into each other at about 115 K; this relates to the overcome blocking temperature of the particles.

It is important to note the role of the measurement time in comparison to the relaxation time of the particle system. We measured the magnetization with a constant heating rate of 3 K min^{-1}. Our experience is that the magnetization curves are independent of the heating rate in the range from 1 to 10 K min^{-1}. Our preferred heating rate is 3 K min^{-1} because on one hand the measurements can be made fast enough and on the other hand the number of data points is high enough.

The relaxation time τ of small single-domain particle systems changes dramatically when reaching the blocking temperature T_B of the particles. Below T_B τ is very long when comparing

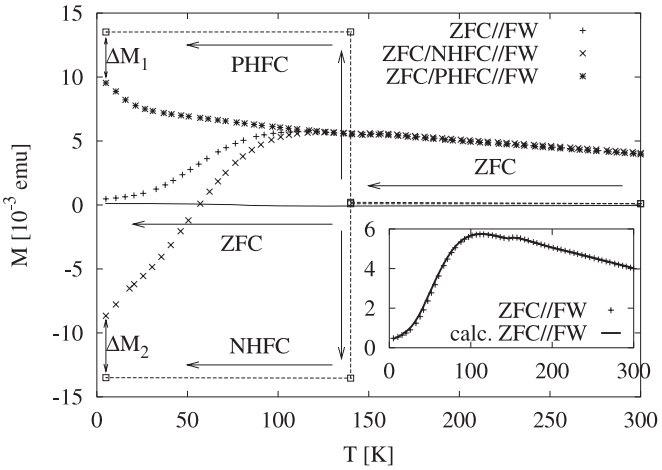

Figure 4. The FW magnetization (Co104) is shown for three different LTMSs prepared in a non-textured sample (ZFC//FW, ZFC/NHFC//FW, ZFC/PHFC//FW). The external field for FW is $B_{\mathrm{FW}} = 50$ mT. The curve in the inset indicated as 'calculated ZFC//FW' is evaluated from the ZFC/PHFC//FW and ZFC/NHFC//FW curves via equation (4). The cooling processes are indicated by arrows. ΔM_1 and ΔM_2 are described in the text.

to the heating time; above it is short. Between 5 and 115 K the measured signal corresponds to a nonequilibrium magnetization depending on the heating rate (here 3 K min^{-1}). At 140 K the liquid starts melting and as a result the particles may rotate, changing the magnetization to slightly higher values due to the forced texture of the particles in the liquid state.

Comparing in figure 4 the magnetization jump ΔM_1 when switching from PHFC to FW (the field from 2 T to 50 mT) with ΔM_2 from NHFC to FW (the field from -2 T to +50 mT) we find $\Delta M_1 \approx \Delta M_2$. This equality indicates that the particles' anisotropy is responsible for these magnetization jumps and particle–particle interaction is negligible. Thus we observe single-particle behaviour in this experiment.

Considering the FW measurement after ZFC in figure 4, the following experimental result is obtained (see inset):

$$\tfrac{1}{2}(M_{\mathrm{ZFC/PHFC//FW}}(T) + M_{\mathrm{ZFC/NHFC//FW}}(T)) = M_{\mathrm{ZFC//FW}}(T). \tag{4}$$

The relationship (4) therefore indicates that there is no difference in the relaxation times when starting by PHFC, NHFC and ZFC prepared low temperature magnetic states. We therefore conclude that only the particle intrinsic anisotropy determines the relaxation rate and not the particle–particle interaction. The influence of the particle–particle interaction on the relaxation rate has recently been described by Hansen and Mørup (1998). In the case of negligible particle–particle interaction each magnetization curve $M_{\mathrm{FC//FW}}(T)$ measured after FC in an arbitrary magnetic field should be 'constructible' from the two limiting cases $M_{\mathrm{ZFC/PHFC//FW}}$ and $M_{\mathrm{ZFC/NHFC//FW}}$ in the sense

$$M^{\star}_{\mathrm{FC//FW}}(T) = \beta M_{\mathrm{ZFC/PHFC//FW}}(T) + (1-\beta) M_{\mathrm{ZFC/NHFC//FW}}(T). \tag{5}$$

β is the fraction of particles in the LTMS corresponding to ZFC/PHFC; β varies between zero and unity. Any deviation from this 'law' must be caused by particle–particle interaction. This result leads us to propose a new method to distinguish between anisotropy and particle–particle interaction measuring the difference $\Delta M = M^{\star}_{\mathrm{FC//FW}} - M_{\mathrm{FC//FW}}$ versus T.

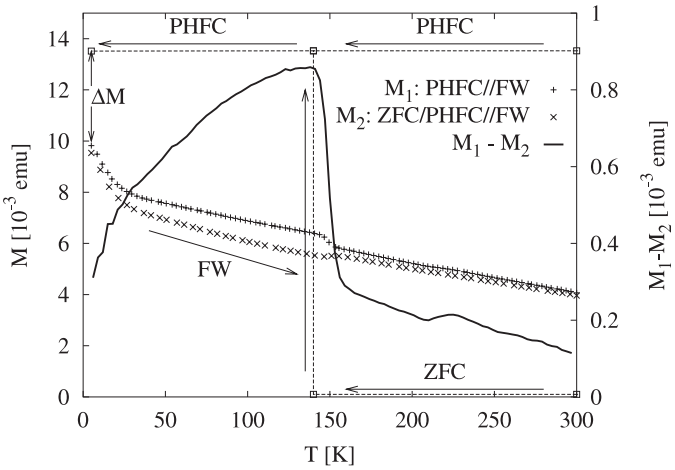

Figure 5. The magnetization of the ferrofluid sample Co104 when heating up from different LTMSs is shown (plus&cross). In the case of ZFC/PHFC//FW (M_2) we have a statistic orientation of the easy axes and aligned moments as LTMS. In the case of PHFC//FW (M_1) the sample should contain particles with oriented easy axes and aligned magnetic moments. $B_{\mathrm{FW}} = 50$ mT. Additionally the magnetization during cooling and the difference $M_1 - M_2$ of the two FW curves is shown. For more details see the text.

In the next step the influence of texture on the most diluted (Co104) sample is investigated. In figure 5 the measured magnetization of the ferrofluid sample when heating up from two different LTMSs is shown. In the non-textured case achieved by applying ZFC/PHFC//FW we expect a statistic orientation of the easy axes and aligned magnetic moments as LTMS. In the other case (PHFC//FW) we expect a textured sample and aligned magnetic moments. Figure 5 shows that the magnetization curve of the PHFC//FW is well above the ZFC/PHFC//FW until the structure of the frozen liquid is broken when the carrier liquid starts melting. In the frozen state the magnetization starts decreasing from the LTMS to lower magnetization due to enhanced thermal activation of the magnetic moments. At 140 K the liquid starts melting and as a result the particles may rotate, changing the magnetization slightly. For the textured sample (PHFC//FW) the preferred orientation of the easy axes gets lost during melting and the magnetization decreases slightly. For the non-textured sample (ZFC/PHFC//FW) the particles tend to align a bit with the external field and we measure a slight increase of the magnetization. Due to the non-zero viscosity of the fluid the magnetization-equality is not reached directly at the melting temperature but at higher temperatures. (This can be explained by the fact that the melting point is a temperature with a defined, relatively high viscosity. Additionally there is a distribution of freezing temperatures for the different molecule chains in the petroleum.)

The ΔM-jump observed in figure 5 after PHFC and switching the high field from 2 T to the 50 mT applied for FW is in both cases (ZFC/PHFC//FW; PHFC//FW) equal and of the order of 30% with respect to the maximal magnetization. We observe practically no difference between the textured and non-textured sample Co104. This is hard to understand for single particles with anisotropy.

For better understanding of the magnetization jumps when changing from PHFC to FW we present a more detailed analysis. Before doing so we show measurements on the non-diluted ferrofluid (Co100) next (figures 6 and 7). Here the same procedures as described for the most diluted sample were applied.

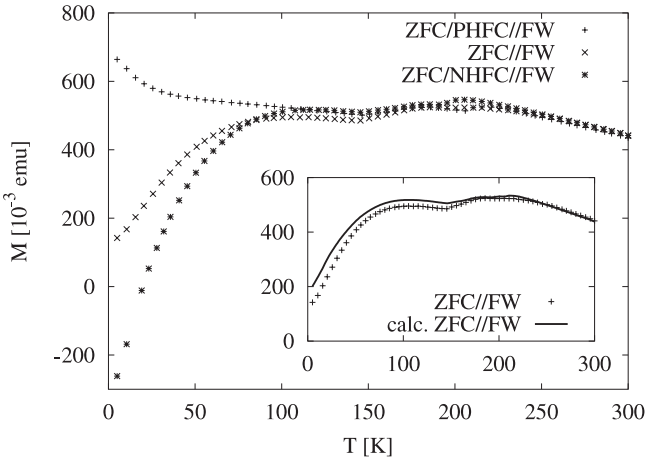

Figure 6. The magnetization during FW in $B_{\mathrm{FW}} = 50$ mT is shown for sample Co100 with three different LTMSs prepared in a non-textured sample (ZFC//FW, ZFC/NHFC//FW, ZFC/PHFC//FW). The inset shows the calculated magnetization (equation (4)) and in comparison the ZFC//FW measurement.

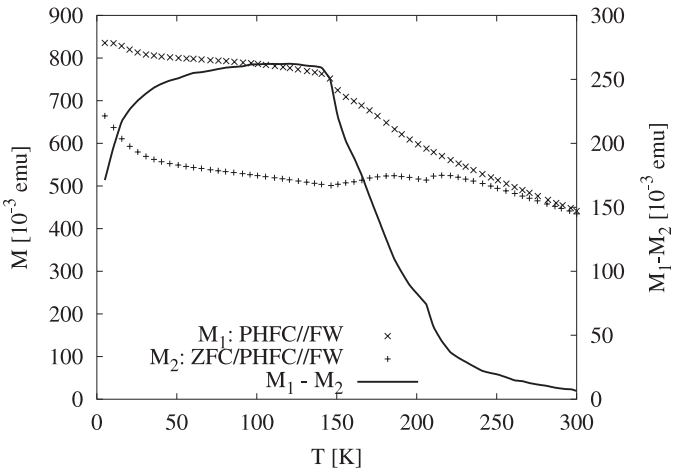

Figure 7. For sample Co100 the measurements PHFC//FW and ZFC/PHFC//FW are shown with $B_{\mathrm{FW}} = 50$ mT. The magnetization of the textured sample lies markedly above the magnetization of the non-textured sample as expected. The difference between both curves is indicated with a separate scale on the right and starts at medium values, exhibits a maximum at the melting temperature and decreases slowly to nearly zero at $T = 300$ K.

In figure 6 the FW magnetization is shown starting from three different LTMSs prepared in the non-textured sample (ZFC//FW, ZFC/NHFC//FW, ZFC/PHFC//FW). The external field for FW is $B_{\mathrm{FW}} = 50$ mT. Again we check the validity of equation (4). The result is plotted as the inset. Here the agreement is not as perfect as in the case of the most diluted sample. So the inset indicates effects which are not caused by the particles' anisotropy.

In figure 7 the FW magnetizations of the Co100 sample in the textured and non-textured states are compared. For this sample the influence of the PHFC process causing the texture is obvious.

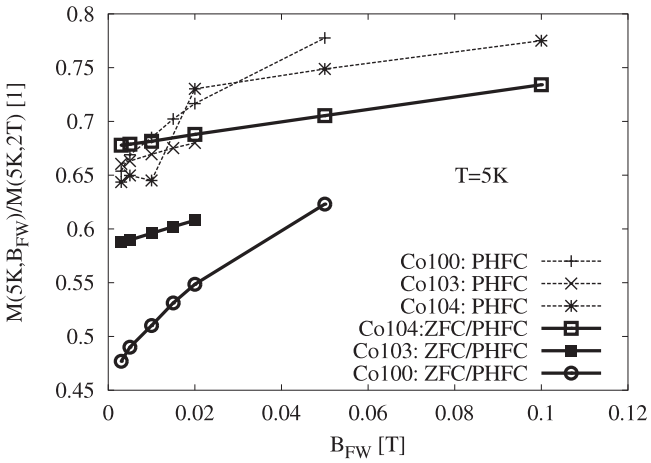

Figure 8. The relative magnetization for $T = 5$ K versus the applied fields B_{FW} is shown. The measurements for the non-textured samples (ZFC/PHFC) can be clearly separated and show a strong dependence on the dilution of the sample. The textured samples (PHFC//FW) all show nearly the same magnetization values.

In figure 8 we plot the measured relative (normalized to the maximum value at $T = 5$ K) magnetization at $T = 5$ K

$$\frac{M(5\ \mathrm{K},\, B_{\mathrm{FW}})}{M(5\ \mathrm{K},\, 2\ \mathrm{T})} =: M_{\mathrm{rel}}^{\mathrm{LTMS}}(B_{\mathrm{FW}}) \tag{6}$$

versus the strength of the external magnetic field during FW for all three samples (Co100, Co103 and Co104). The textured (LTMS prepared by PHFC) and non-textured samples (LTMS prepared by ZFC/PHFC) are compared.

What do we expect for ideal Stoner–Wolfarth particles? In the case of statistically oriented particles and in consequence easy axes we expect for the limiting case $B_{\mathrm{FW}} \to 0$ the value $M_{\mathrm{rel}}^{\mathrm{ZFC/PHFC}}(B_{\mathrm{FW}})$ to tend to 0.5. On the other hand in the ideal case of perfect texture through PHFC $M_{\mathrm{rel}}^{\mathrm{PHFC}}(B_{\mathrm{FW}} \to 0)$ is expected to be unity because the magnetization vectors cannot jump over the energy barrier in the minimum belonging to the negative direction (no sufficient thermal energy at $T = 5$ K).

Whereas the non-textured samples show a clear systematic change with the most diluted sample exhibiting the smallest magnetization jump all textured samples (within the scatter of the measurements) show no influence of concentration (dilution). The sample Co104 is the sample with the least expected influence of interaction. But the normalized magnetization is not 0.5 as predicted but approximately 0.68. This can only be due to the fact that the magnetization vector cannot fall into the deepest energy minimum after PHFC. This may be the effect of additional local minima in the energy curve of the ideal Stoner–Wohlfarth-particle which may be caused by the surface. The sample Co103 shows a bigger magnetization jump than the most diluted sample (Co104). This effect must be due to the enhanced interaction through the higher packing density. The magnetization is less for this higher packing density. This may be explained with complex interaction models but we focus on the simplest one that can explain this effect: the magnetic nanoparticles partly tend to build dimers when the packing density gets higher. In the high field the dimer structure has the maximal possible magnetization. In low fields the particles tend to lower their common stray field by turning the magnetization of one particle opposite to the other. The resulting magnetization of such

dimers is nearly zero. This model can explain the lower relative magnetization with increasing packing density in untextured samples (ZFC/PHFC//FW).

The curves of relative magnetization for PHFC//FW cannot be separated versus concentration within the scatter of the measurement. This nearly dilution independent behaviour shows, that the particles tend to agglomerate (in our simplest model to dimers). Instead of showing no magnetization jump as predicted for the ideal textured case, the relative magnetization lowers to a value of approximately 0.65. The explanation is nearly the same as in the case of dense ferrofluids with statistical distribution of the anisotropy axes: in the fluid state and an external field of 2 T the particles tend to build agglomerates and are fixed in this position below 150 K. When reducing at 5 K the field to the measurement field the effective magnetization of these agglomerates reduces to nearly zero.

Next we will try to get some quantitative information about this interaction. After a short introduction to the susceptibility we consider experiments performed on the most diluted sample (Co104) in the non-textured and textured states.

5. Laboratory susceptibility

To obtain information about interactions in a magnetic system the so-called laboratory susceptibility can be used (see Hesse *et al* 2000 for full details). The susceptibility in field B is defined by

$$\chi(B,T) = \mu_0 \frac{\partial M}{\partial B} = \mu_0 \lim_{\Delta B \to 0} \left[\frac{M(B+\Delta B,T) - M(B,T)}{\Delta B} \right]_{B=\text{constant}}. \quad (7)$$

For the calculation of the laboratory susceptibility χ_{lab} we replace the limit $\Delta B \to 0$ by a small difference ΔB of two adjacent magnetization curves ($B_1 = B$, $B_2 = B + \Delta B$):

$$\chi_{\text{lab}}(B,T) = \mu_0 \left[\frac{M(B_2,T) - M(B_1,T)}{\Delta B} \right]_{B=(B_1+B_2)/2}. \quad (8)$$

In practice this means that we make two (or more) temperature dependent measurements in different but adjacent fields B_{FW}, subtract them from each other and divide them by the field difference $B_2 - B_1 = \Delta B$.

For a paramagnetic system consisting of small particles with magnetic moments of the order of thousands of μ_{B}, the susceptibility exhibits a maximum in moderate temperature and field ranges. The temperature belonging to the maximum of the susceptibility is (in the case of noninteracting superparamagnetic particles) only dependent on the external field B and the magnetic moment μ of the particles.

For the laboratory susceptibility maximum value the following equation holds ($\alpha = 1.911\,181\,737$ (for the calculation of α see Hesse *et al* 2000) and k_{B} is the Boltzmann constant):

$$\alpha k_{\text{B}} T(\chi_{\max}) = \mu B. \quad (9)$$

We take the magnetization curves derived from a quasi-paramagnetic LTMS (reached by ZFC/PHFC, figure 9) to calculate the laboratory susceptibility of the sample and get by extrapolating the results to high fields the mean value for the magnetic moment and in consequence the radius of the nanoparticles. Figure 10 shows the evaluated values for χ_{lab}.

It is possible to determine the magnetic moment of the nanoparticles from the easy to distinguish temperature belonging to the maximum of the susceptibility. The magnetic moment seen by this method varies with B. This may be explained by the following facts: the theory holds for superparamagnetic particles without anisotropy and interaction. The Co particles do have anisotropy and the particles will interact at least a little. But in the case of high fields

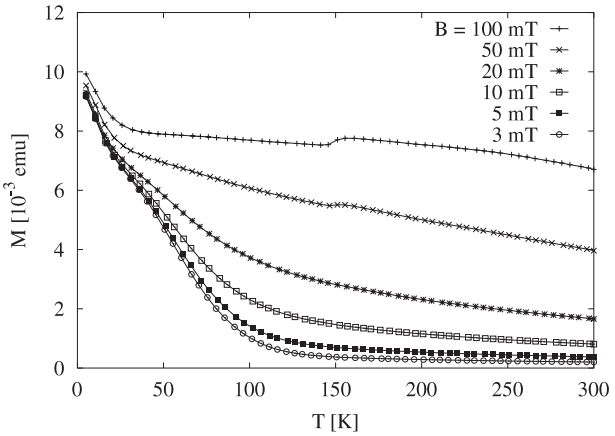

Figure 9. Magnetization measurement after ZFC/PHFC in the indicated fields B_{FW} (sample Co104). The induced texture at the melting point gets visible through the small increase of the magnetization at $T = 140$ K for fields higher than 20 mT.

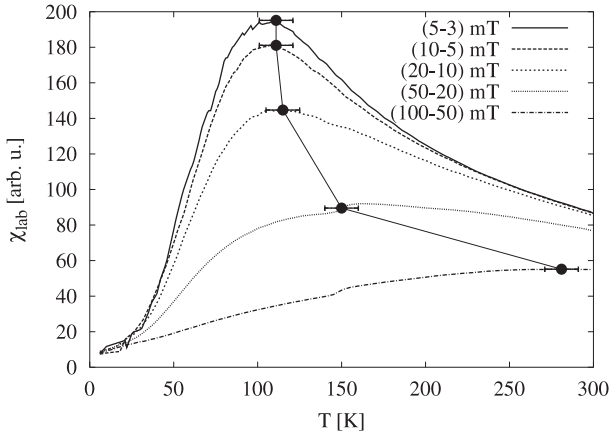

Figure 10. The laboratory susceptibility was calculated with equation (8) from the adjacent magnetization curves presented in figure 9. The maxima of the curves are indicated together with an error estimation for the maximum's temperature. As in the ideal case, the susceptibility curves start at very low values (in the ideal case at $\chi = 0$), exhibit a maximum and decrease with higher temperatures. The deviation from the ideal superparamagnetic behaviour is discussed and interpreted in the following figure.

B, the anisotropy energy and the interaction energy become negligible in comparison to the Zeeman energy $M_0 V B$ and one gets as extrapolation the 'real' value of the particles' magnetic moment. With a rather simple heuristic approach we are able to determine this disturbing field B_{dist}. The idea is as follows: the magnetic moment of each particle experiences a (local) magnetic field. This field is a vector sum of the externally applied field and the disturbing field.

This disturbing magnetic field B_{dist} in principle has two components $B_{\mathrm{dist}\parallel}$ and $B_{\mathrm{dist}\perp}$ with respect to the applied field. We describe the thermal expectation value of the magnetic moment in the direction of the external magnetic field as given by the Langevin function belonging to the resulting magnetic field $B_{\mathrm{res}} = \sqrt{(B_{\mathrm{ex}} + B_{\mathrm{dist}\parallel})^2 + (B_{\mathrm{dist}\perp})^2}$. In a magnetization measurement

the projection of the magnetic moment on the direction defined by the applied external magnetic field is measured, where $\cos(\vartheta) = \frac{B_{ex}+B_{dist\|}}{B_{res}}$ and ϑ is the projection angle. So we obtain for the thermal expectation value of the particles' magnetic moment $\mu(T)$ when $\mu = \mu(T = 0)$

$$\mu(T) = \mu \frac{B_{ex} + B_{dist\|}}{B_{res}} \left[\coth\left(\frac{\mu B_{res}}{k_B T} \right) - \frac{k_B T}{\mu B_{res}} \right]. \tag{10}$$

In a first approximation, when the relation $|B_{ex}| > |B_{dist}|$ holds, we obtain

$$\mu(T) = \frac{\mu B_{ex}}{\sqrt{B_{ex}^2 + (B_{dist\perp})^2}} \left[\coth\left(\frac{\mu\sqrt{(B_{ex})^2 + (B_{dist\perp})^2}}{k_B T} \right) - \frac{k_B T}{\mu\sqrt{(B_{ex})^2 + (B_{dist\perp})^2}} \right]. \tag{11}$$

When $B_{dist\perp}$ is caused by the dipole interaction it is expected that its influence will be visible in the frozen state and becomes practically negligible in the liquid state of the ferrofluid. We assume that we can use a similar ansatz for the magnetization of the particles ensemble of the frozen ferrofluid, it can be considered as an approximation for the much more exact considerations presented by Garcia-Palacios (2000):

$$M(T) = \frac{M(T = 0) B_{ex}}{\sqrt{B_{ex}^2 + \langle B_{dist\perp}^2 \rangle}} \left[\coth\left(\frac{\mu\sqrt{B_{ex}^2 + \langle B_{dist\perp}^2 \rangle}}{k_B T} \right) - \frac{k_B T}{\mu\sqrt{B_{ex}^2 + \langle B_{dist\perp}^2 \rangle}} \right]. \tag{12}$$

Because there is some success in fitting experimental data using equation (12) the disturbing field must be considered as an average value being a typical characteristic feature of the particle ensemble. Therefore we labelled it $\langle B_{dist\perp}^2 \rangle$ as a mean square of a disturbing field, knowing that to date there is no theoretical justification for it.

The maximum condition for the susceptibility versus T regarding the disturbing field may be calculated. With the ansatz $\langle B_{dist\perp} \rangle^2 = (b B_{ex})^2$ ($b \geqslant 0$), we get the following results:

$$\alpha k_B T(\chi_{max}) = \mu B_{ex} \sqrt{1 + b^2}. \tag{13}$$

We execute the evaluation in the following manner: in a first step equation (9) is used to evaluate the field dependent particles' magnetic moment $\mu(B_{ex})$ for each magnetic field B_{ex}. These $\mu(B_{ex})$ values are plotted against the external field B_{ex}. One can 'see' with this simple plot the value μ_{real} which is reached for high fields. In the sample considered (Co104) the temperature for the susceptibility maximum corresponds to the liquid state where we expect $B_{dist\perp} \approx 0$. In the second step we take the correction equation (13)

$$\mu(B_{ex}) = \mu_{real} \sqrt{1 + \left(\frac{B_{dist\perp}}{B_{ex}} \right)^2} \tag{14}$$

and fit it to the uncorrected values from the first step. By this fit one gets the extrapolated magnetic moment μ_{real} and the mean disturbing field in the sense of $\sqrt{\langle B_{dist\perp}^2 \rangle} = B_{dist\perp}$ (figure 11).

Figure 11 shows the results of the calculations and a high field extrapolation which yields a value of $\mu_{real} = 8500 \pm 500\ \mu_B$. This corresponds to a mean radius of the particles of approximately 2.4 nm assuming that the particles are spherical and of hexagonal cobalt without any further corrections. The disturbing field evaluated from the fit is $B_{dist\perp} = 36 \pm 5$ mT.

This new method was also applied to the same particle system after the positive high field cooling sequences. The difference between the two experiments was only the LTMS of the system: textured or non-textured quasi-paramagnetic LTMS. While it seems clear that the particles' magnetic moment may not change with the measurement method, the disturbing field may of course be influenced by the spatial arrangement of the particles. But the evaluation of the experimental data shows in both cases nearly the same results: the magnetic moment

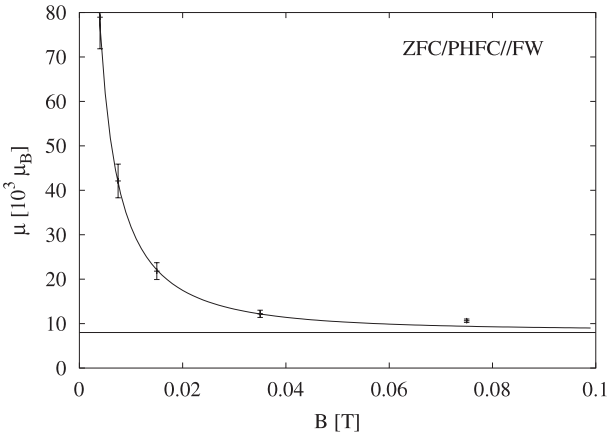

Figure 11. Magnetic moments of the nanoparticles estimated from the laboratory susceptibility maxima and high field extrapolation (equation (14)) plotted versus the field B_{mean}. The calculations result in a mean radius of 2.4 nm or a magnetic moment of $8500 \pm 500\ \mu_{\text{B}}$ and a disturbing field $B_{\text{dist}\perp} = 36 \pm 5$ mT.

is calculated to be 8400 respectively 8500 μ_{B} and the disturbing field is in this approach in both cases 36 mT (the field has an error of about ± 5 mT; the error for the magnetic moment is $\pm 500\ \mu_{\text{B}}$). This result shows that it was practically impossible to texture the very diluted sample in the ideal sense by PHFC. But the value of 8500 μ_{B} shows that we are not dealing with 'big' particle ensembles that may be formed by clustering of the nanoparticles because this magnetic moment corresponds to a radius of only 2.4 nm (in agreement with the 'magnetic radius' calculated from room-temperature magnetization measurements).

The maximum of $\chi_{\text{lab}}(T)$ can be used as an additional proof that we have no collective behaviour of the particles in our sample. The averaged disturbing field was determined for the other samples too and it was found that there is a small increase of the field for higher concentrations of the ferrofluid: 40 mT for sample Co103 and 49 mT for sample Co100.

Therefore, we conclude that independently of ZFC or PHFC in the liquid ferrofluid a fraction of the particles is arranged in agglomerates, in the simplest case dimers. The disturbing field found by the analysis presented above is of the proper order to originate from dipole–dipole interaction for particles lying as close as the organic hull allows (approximately 2 nm; the distance of the particles' midpoints is 9 nm).

6. Summary and conclusions

We have presented and compared different novel strategies for magnetization measurements applicable to nanosized single-domain particle systems and used them to obtain information about magnetic properties of frozen Co-based ferrofluids.

In a first step we gained information about the mean size and size distribution of the nanoparticles by transmission electron microscopy (TEM). In a second step, we presented various possibilities for preparing well defined low temperature magnetic states by cooling the sample with and without applied external magnetic fields. Starting from liquid ferrofluids this allows us to prepare non-textured or textured samples in the sense of preferred oriented easy directions for particle magnetizations. The influence of the different low temperature magnetic states on the field-warming curve in magnetization measurements was discussed and

applied. In the case of the Co-based ferrofluids investigated here the measurement results can be interpreted in a way that predicts single-particle behaviour for particles in highly diluted ferrofluids frozen in a zero magnetic field. When a magnetic field is applied in the liquid state of the ferrofluid, the particles tend to agglomerate partially and build dimers or more complicated clusters, turning their easy axes parallel to the magnetic field. We have shown that in diluted samples from the limiting cases of low temperature magnetic states reached by ZFC/NHFC as well as by ZFC/PHFC each ZFC//FW (secondary cooling in arbitrary DC magnetic fields) magnetization curve can be constructed.

Third, we tried to determine the particle–particle interaction quantitatively using the susceptibility maximum when measuring versus temperature. The susceptibility shows a maximum which depends in the case of ideal superparamagnets only on the particles' magnetic moment and the external field B. The observed field dependence of the magnetic moment determined by the maximum of the susceptibility could be explained in a simple and easy to use model including an additional field $B_{\mathrm{dist}\perp}$ which changes with the particle–particle interaction. The mean value of the particles' moment is in good agreement with the direct measurement of the sizes via TEM and evaluation from room temperature magnetization measurements.

The presented ways to prepare definite low temperature magnetic states and the followed magnetization measurements open a large field for achieving new measurement results. They are applicable for artificial regular particle arrays too, and in consequence open new possibilities for simulation (e.g. Monte Carlo simulation, Verdes *et al* 2002) and for the application of relaxation models. With these techniques, it should be possible in future to derive more information from the easy to measure magnetization curves, distinguishing between the influences of anisotropy and particle–particle interaction. We hope that we could encourage experimentalists and theoreticians to use more refined magnetization measurements as an easy possibility to gain deeper information about nanoparticle systems.

Acknowledgments

We are grateful to Dr K Weyand, Physikalisch Technische Bundesanstalt Braunschweig, for granting us access to the SQUID magnetometer facility in his laboratory. Our thanks go to Dr C Gansau and Dr N Buske from the BerlinHeart AG for supplying us with the ferrofluid.

OM would like to thank Dr O Hupe for help during the time at the TU Braunschweig.

References

Abu-Aljarayesh I, Al-Jamel A F and Said M R 2002 *Physica* A **321** 82–6
Bakuzis A F, Da Silva M F, Morais P C, Olavo L S F and Skeff N K 2000 *J. Appl. Phys.* **87** 2497–502
Berkov D V, Görnert P, Buske N, Gansau C, Mueller J, Giersig M, Neumann W and Su D 2000 *J. Phys. D: Appl. Phys.* **33** 331–7
Blums E, Cebers A and Maiorov M M 1997 *Magnetic Fluids* (Berlin: de Gruyter)
Brown W F 1963 *Phys. Rev.* **130** 1677–86
Chantrell R W, Bradbury A, Popplewell J and Charles S W 1982 *J. Appl. Phys.* **53** 2742–4
Denisov S I, Nefedchenko V F and Trohidou K N 2000 *J. Phys.: Condens. Matter* **12** 7111–5
Eberbeck D and Ahlers H 1999 *J. Magn. Magn. Mater.* **192** 148–58
Fannin P C 2002 *J. Magn. Magn. Mater.* **252** 59–64
Fannin P C, Scaife B K P and Charles S W 1988 *J. Phys. D: Appl. Phys.* **21** 1035–6
Garcia-Palacios J L 2000 *Adv. Chem. Phys.* **112** 1–210
Hansen M F and Mørup S 1998 *J. Magn. Magn. Mater.* **184** 262–74
Hesse J, Bremers H, Hupe O, Veith M, Fritscher E W and Valtchev K 2000 *J. Magn. Magn. Mater.* **212** 153–67
Hesse J, Pütter S, Michele O, Bremers H, Hupe O, Hartung H and Eichler M 2002 *Phys. Status Solidi* a **189** 481–94
Hupe O, Chuev M A, Bremers H, Hesse J and Afanas'ev A M 1999 *J. Phys.: Condens. Matter* **11** 10545–56

Kachkachi H, Noguès M, Tronc E and Garanin D A 2000 *J. Magn. Magn. Mater.* **221** 158–63
Koksharov Yu A 2000 *J. Appl. Phys.* **88** 1587–92
Luo W, Nagel S R, Rosenbaum T F and Rosensweig R E 1991 *Phys. Rev. Lett.* **67** 2721–4
Néel L 1949 *Ann. Geophys.* **5** 99
Neuringer J L and Rosensweig R E 1964 *Phys. Fluids* **7** 1927–37
Pathmamanoharan C and Philipse A P 1998 *J. Colloid Interface Sci.* **205** 340–53
Peng D L, Hihara T, Sumiyama K and Morikawa H 2002 *J. Appl. Phys.* **92** 3075–83
Stamps R L 2002 *J. Magn. Magn. Mater.* **242–245** 139–45
Stoner E C and Wohlfarth E P 1948 *Phil. Trans. R. Soc.* A **240** 599–642
Verdes C, Ruiz-Diaz B, Thompson S M, Chantrell R W and Stancu Al 2002 *Phys. Rev.* B **65** 174417
Weser T and Stierstadt K 1985 *Z. Phys.* B **59** 253–6
Williams H D, O' Grady K and El Hilo M 1993 *J. Magn. Magn. Mater.* **122** 129–33
Zahn M and Shenton K E 1980 *IEEE Trans. Magn.* **16** 387–415